Applied Catalysis B: Environmental 125 (2012) 158–165

Contents lists available at SciVerse ScienceDirect

Applied Catalysis B: Environmental

journal homepage: www.elsevier.com/locate/apcatb

Study on the mechanism of the oxidation of soot on Fe_2O_3 catalyst

Steffen Wagloehner, Sven Kureti*

Technical University of Freiberg, Department of Energy Process Engineering and Chemical Engineering, Fuchsmühlenweg 9, D-09596 Freiberg, Germany

ARTICLE INFO

Article history:
Received 24 January 2012
Received in revised form 10 May 2012
Accepted 24 May 2012
Available online 1 June 2012

Keywords:
Soot oxidation
Fe_2O_3 catalyst
Mechanism
Isotopic labelling

ABSTRACT

The present paper deals with the mechanism of the soot oxidation on Fe_2O_3 catalyst. The catalytic oxidation of soot is essential for the regeneration of diesel particulate filters already applied for vehicles and working machines. A series of mechanistic studies were conducted including systematic variation of reaction conditions, isotopic labelling ($^{18}O_2$) and local temperature measurements by using an IR camera. These investigations provided knowledge on the transfer of oxygen from the gas-phase to catalyst and soot, the heat distribution on the surface of the catalyst/soot mixture and the effect of crucial parameters on the kinetics, i.e. heating rate, contact mode (tight vs. loose) and catalyst/soot ratio. From these examinations the following insights were derived: (1) Lattice oxygen of Fe_2O_3 is drastically involved in the soot oxidation by migration from the bulk to the soot. Therefore, the ratio of catalyst/soot directly affects the total amount of oxygen transported from catalyst to soot. (2) In another route, oxygen is "pumped" from the gas-phase via the Fe_2O_3 surface to the soot. (3) The oxygen transfer from Fe_2O_3 to soot mainly occurs by physical contact points. (4) The local temperature in the catalyst/soot mixture strongly depends on the amount and heat capacity of the catalyst, respectively, i.e. the catalyst acts as a temperature buffer. Thus, an optimum ratio of catalyst/soot exists reflecting a compromise of high number of contact points (high catalyst mass) and low heat capacity (low catalyst mass).

Consequently, a global reaction mechanism of the catalytic soot oxidation on Fe_2O_3 was suggested. This mechanism implies the formation of oxygen defect sites as a result of the oxygen transfer to the soot. These defect sites are refilled either by migration of surface oxygen and re-oxidation by gas-phase oxygen, respectively, or by bulk oxygen. The resulting oxygen deficiency of the bulk is balanced by migration of oxygen from the surface or sub-surface.

1. Introduction

For the removal of soot from the exhaust of diesel engines so called diesel particulate filters (DPF) are currently applied. These filters operate with high efficiency by forcing the exhaust to flow through their porous walls [1]. However, DPF systems require a regeneration step, since soot deposits can produce substantial backpressure leading to rise of fuel consumption.

The preferred method of DPF regeneration is the CRT technology (continuously regenerating trap) involving the oxidation of soot by NO_2 and O_2. The required NO_2 is produced by catalytic oxidation of NO on Pt. The catalyst is applied as a coating on the DPF or in form of diesel oxidation catalyst (DOC) located upstream to the DPF. In the former procedure, NO is recycled several times along the DPF thus accelerating the regeneration process [2]. In CRT, soot is mainly oxidised into CO_2, whereas NO_2 is reduced to form NO. The optimum operation window of CRT ranges from 200 to 450 °C. At lower temperatures the rate of soot oxidation is not sufficient, whereas above 450 °C the formation of NO_2 is determined by thermodynamics [3]. The role of NO_2 is to initiate the soot/O_2 reaction by rapidly forming reactive surface complexes [4]. These surface oxygen compounds (SOC) react with O_2 to produce very unstable surface species which decompose or undergo further oxidation by O_2.

In contrast to heavy duty vehicles, the CRT technique is not effectual for passenger vehicles due to their rather low molar NO_x/C ratio (<10 on average). Thus, DPF systems of passenger cars require an additional regeneration process. A suitable method already applied is the post-injection of fuel resulting in huge emissions of HC, CO and H_2. These components are oxidised on the DOC rising the temperature of DPF up to ca. 750 °C. This temperature is adequate to rapidly oxidise the soot by gas-phase oxygen [5].

An alternative technique currently employed as well is the use of so called fuel borne catalysts (FBC) [1]. FBC systems represent metal organic compounds based on Ce or Fe, e.g. ferrocene, and are added to the fuel [5]. Fuel borne catalysts decrease the engine output of soot by directly oxidising the soot in the combustion chamber. Additionally, they are embedded in the soot particles in highly dispersed manner thus initiating the soot oxidation already at approx. 300 °C. However, after removal of the soot the fuel borne catalysts

* Corresponding author. cc.
E-mail address: kureti@iec.tu-freiberg.de (S. Kureti).

0926-3373/$ – see front matter © 2012 Elsevier B.V. All rights reserved.
http://dx.doi.org/10.1016/j.apcatb.2012.05.032

remain in form of loose ash entities being suspected to increase the DPF backpressure.

Furthermore, the ignition temperature of soot can be reduced by the CDPF technique which implies a catalytic DPF coating accelerating the soot/O_2 reaction. The efficiency of this process is closely associated with tight contact between the soot deposited and the catalytic coating. Indeed, in CDPF loose contact mostly predominates resulting in a rather limited benefit of the catalyst [6]. A series of catalytic materials, mainly transition metal oxides and rare earth metal oxides, were tested for soot oxidation [7–12]. Particularly, iron oxides were reported to be effective [13–16].

In this context, the aim of the present work was to contribute to the understanding of the fundamentals of the soot oxidation on iron oxide catalysts. For this purpose, α-Fe_2O_3 was used as model catalyst being the thermodynamically favoured modification under diesel exhaust conditions. The studies included the effect of different reaction parameters on the kinetics of soot oxidation, the evolution of the local temperature of the catalyst/soot mixture as well as the role of the catalyst in the transfer of oxygen to the soot.

2. Experimental

2.1. Preparation and characterisation of Fe_2O_3 catalyst and soot

The α-Fe_2O_3 model catalyst was synthesised by polyvinyl alcohol (PVA) method as reported in detail elsewhere [17]. Briefly, the aqueous solution of $Fe(NO_3)_3$ and PVA with a molar Fe/VA ratio of 2 was boiled down and the resulting residual was calcined in air at 600 °C for 5 h. The crystalline structure of the catalyst was confirmed by PXRD (D8 Advance, Bruker) using Ni filtered Cu Kα radiation. The BET surface area was investigated by multi-point Sorptomatic 1990 (Porotec) using N_2 as adsorbate. The sample was pre-treated at 300 °C for 2 h in vacuum (10^{-4} mbar) and cooled to −196 °C, and then the isotherm was recorded. From the adsorption data recorded at p/p_0 ratios between 0.05 and 0.30 the BET surface area was derived. The BET surface area of the α-Fe_2O_3 catalyst was determined to be 15 m^2/g.

The soot was prepared by burning a C_3H_6/O_2 mixture in a diffusion flame and was separated from the exhaust by employing a particulate filter as reported recently [18]. The most important physical–chemical properties of the soot collected are as follows: BET surface area: 90 m^2/g, amount of adsorbed species: 4 wt.% (each ca. 50 wt.% H_2O and hydrocarbons), chemical composition (adsorbed species neglected): 97.5 wt.% C, 1.5 wt.% O, 0.6 wt.% H, 0.2 wt.% N, soot is ashless, mean diameter of primary particles: 45 nm.

2.2. Temperature programmed oxidation

The effect of selected reaction parameters on the kinetics of the catalytic soot oxidation was investigated by using the temperature programmed oxidation (TPO). In TPO, the temperature was linearly increased from room temperature to 500 °C. The examinations included the systematic variation of contact mode, catalyst/soot ratio and heating rate. The total gas flow was kept at 500 ml/min (STP), while the composition of the feed was adjusted by independent flow controllers (MKS Instruments). Effluenting CO and CO_2 were analysed by a non-dispersive infrared spectrometer (Binos 1.2, Leybold-Heraeus). The experiments were performed with a catalyst/soot mixture implying an amount of 0.375–20 mmol catalyst and 5 mmol soot. The heating rate was varied from 1.8 to 10 K/min. Both solids were mixed by using two different procedures. Loose contact mixture was established by shaking catalyst and soot in a glass vial (24 mm × 52 mm), while tight contact was prepared by ball milling. For the later, catalyst and soot were milled for 15 min employing a Pulverisette 0 (Fritsch) with a hardened steel ball (m = 940 g). After mixing, the respective blend was pressed for 2 min at 4 MPa, granulated and sieved to a mesh of 125–250 μm to avoid discharge in the catalytic tests. Former investigations demonstrated that pressing and granulating do not affect the activity of the mixture, whereas the grinding procedure was found to be the crucial step of preparation [19]. Finally, the catalyst/soot mixture was placed in the quartz glass tube reactor (i.d. 10 mm) as packed bed fixed by quartz wool. The gas temperature was monitored by two K-type thermocouples; one was located directly in front of and the other behind the bed. In some experiments the temperature was additionally measured in the catalyst/soot bed using a K-type micro-thermocouple with a diameter of 0.2 mm.

2.3. Temperature distribution in the catalyst/soot mixture

The development of the local temperature of the catalyst/soot mixture was investigated by using an IR camera. A TPO was performed in a special stainless steel reactor (i.d. 10 mm) implying a sapphire window located above the packed bed. The temperature of the surface of the catalyst/soot bed was recorded by a Pyroview 380M camera (DIAS). The TPO was made by taking a blend of 10 mmol Fe_2O_3 and 5 mmol soot being in tight contact mode. As in standard TPO (Section 2.2) the feed consisted of 10 vol.% O_2 and 90 vol.% N_2 at a total flow of 500 ml/min (STP); the heating rate was 8.6 K/min.

2.4. Isotopic studies

In the isotopic TPO investigations $^{18}O_2$ labelled oxygen (Campro Scientific) was used to investigate the oxygen transfer from the catalyst to soot [19]. To reduce the amount of $^{18}O_2$ the reaction conditions were modified as compared to those described in Section 2.2. The feed contained 2270 vppm $^{18}O_2$ using N_2 as balance, while supplying a total flow of 500 ml/min (STP). The temperature was increased from 200 °C to 1000 °C with a ramp of 20 K/min. The quantity of soot was always kept at 0.3 mmol, whereas the molar ratio of Fe_2O_3/soot was between 0.5 and 2 adjusting tight and loose contact mode. For the isotopic TPO a quartz glass tube reactor (i.d. = 8 mm) was taken and the gas-phase analysis was carried out by chemical ionisation mass spectrometry (Airsense 500, MS4).

Furthermore, a HTPR study (temperature programmed reduction by H_2) was subsequently performed to determine the amount of gas-phase oxygen taken up by the catalyst upon TPO. After TPO, the catalyst was cooled to 200 °C in N_2 and was then exposed to a mixture of 10 vol.% H_2 and 90 vol.% Ar. Finally, it was heated with a ramp of 20 K/min to 1000 °C.

3. Results and discussion

3.1. Variation of the conditions in soot oxidation on Fe_2O_3 catalyst

3.1.1. Variation of the contact mode of the catalyst/soot mixture

The CO_2 profiles of the TPO studies performed with loose and tight contact mixture of Fe_2O_3 catalyst and soot are depicted in Fig. 1, whereas the CO and CO_2 traces of bare soot are also included. Note that in the absence of the catalyst the soot was diluted with quartz wool to avoid strong exothermal effects and hot spots, respectively. The TPO of the tight contact mixture provides a clear CO_2 peak with a maximum concentration of 7.5 vol.% at approx. 410 °C. In loose contact mode CO_2 formation is shifted to higher temperatures and appears over an extended temperature range (400–650 °C) with a maximum at ca. 585 °C and a broad shoulder at 500 °C. Consequently, the CO_2 content is clearly lower as referred

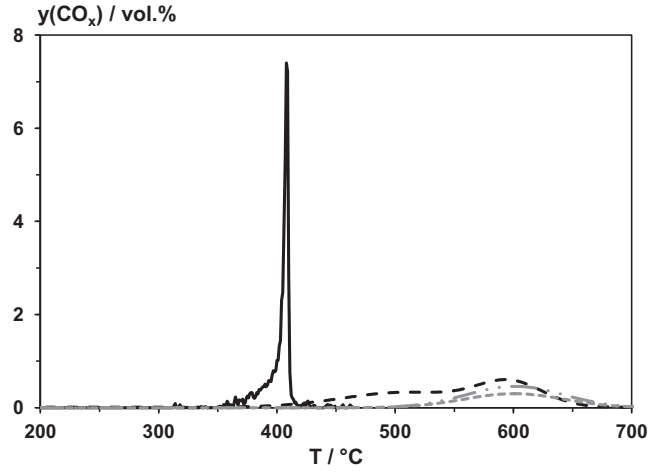

Fig. 1. CO_2 profiles of TPO studies performed with Fe_2O_3/soot mixture in tight (—) and loose contact mode (–) as well as CO (▬) and CO_2 (—··—) profile of TPO of bare soot. Conditions: $n(Fe_2O_3)$ = 10 mmol (if present), n(soot) = 5 mmol, $y(O_2)$ = 10 vol.%, $y(N_2)$ = 90 vol.%, β = 3.3 K/min, F = 500 ml/min (STP).

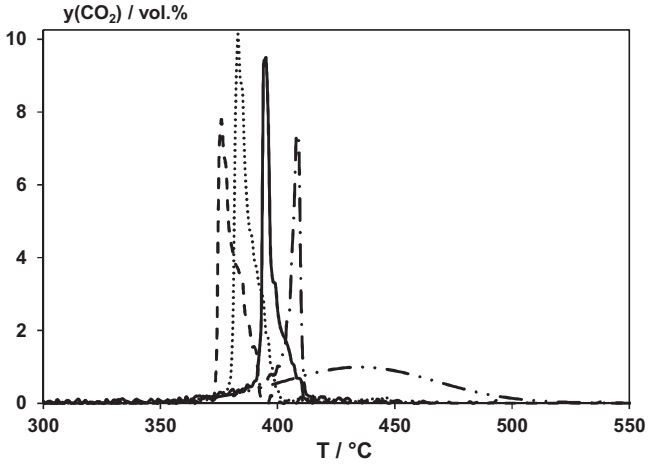

Fig. 2. CO_2 profiles of TPO studies performed with Fe_2O_3/soot mixture in tight contact mode using 1.25 (-.-), 2.5 (···), 5 (—), 10 (—·—) and 20 mmol Fe_2O_3 (—··—). Conditions: n(soot) = 5 mmol, $y(O_2)$ = 10 vol.%, $y(N_2)$ = 90 vol.%, β = 3.3 K/min, F = 500 ml/min (STP).

to that of the tight contact mixture. For both types of catalyst/soot mixtures no CO output is found being associated with the high CO oxidation activity of the Fe_2O_3 catalyst [14,15,20]. However, in TPO of bare soot significant proportion of CO is formed as expected from literature [14] and the CO and CO_2 production appears in the same temperature regime as for the high temperature CO_2 signal (585 °C) of the loose contact blend. Therefore, we attribute the later feature to the non-catalytic oxidation of soot. Contrary, the CO_2 shoulder at 500 °C observed for the loose contact mixture is ascribed to the catalytic soot conversion.

The drastic difference in the performance of loose and tight contact mixture is typical for non-mobile catalysts such as Fe_2O_3 and Co_3O_4 [6,21]. As former studies suggest that the role of Fe_2O_3 lies in the transfer of oxygen to the soot by physical contact points [14,22], it is evident that the distance of Fe_2O_3 catalyst and soot particles and the number of contact points, respectively, is a crucial feature. Simonsen et al. [12] recently showed the migration of soot particles to non-mobile catalysts upon oxidation. Obviously, in tight contact mode the distance between catalyst and soot is rather small including a multitude of contact points, but for increasing distance, i.e. loose contact, the bridging of this gap becomes more and more rate determining.

3.1.2. Variation of the molar ratio of catalyst and soot

The effect of the catalyst on the kinetics of soot oxidation was further studied by varying the proportion of Fe_2O_3 from 0.375 to 20 mmol, whereas the initial abundance of soot was kept at 5 mmol. The studies were only performed for tight contact mixtures. The TPO data of the catalyst/soot blends with 1.25–20 mmol Fe_2O_3 are depicted in Fig. 2 evidencing the strong effect of the catalyst amount on the rate of CO_2 production. Interestingly, in this series the mixture with the highest amount of Fe_2O_3 (20 mmol) shows the lowest activity as indicated by highest temperature of maximum CO_2 content ($T_{CO2,max}$ = ca. 430 °C) and a broad CO_2 trace. When reducing the amount of catalyst the CO_2 profile gets sharper and $T_{CO2,max}$ decreases continuously, e.g. for 1.25 mmol Fe_2O_3 the maximum CO_2 concentration appears at 375 °C already. These findings are substantiated by the temperature of the catalyst/soot bed clearly showing increasing jump in temperature with decreasing amount of catalyst (Fig. 3). The TPO with 20 mmol Fe_2O_3 exhibits a difference between inlet and peak bed temperature of ca. 35 K during maximum CO_2 formation, while with 10 mmol it is ca. 60 K and with 2.5 mmol it is even ca. 160 K. This temperature rise is ascribed to the heat evolution of the exothermic CO_2 production (for carbon oxidation: $\Delta H = -393$ kJ/mol). Since the initial amount of soot and total gas flow is kept constant, the temperature rise depends on the heat capacity of the packed bed. Thus, it is obvious that the quantity of Fe_2O_3 affects the heat evolution in the catalyst/soot mixture, which directly influences the rate of soot oxidation [23].

However, as shown in Fig. 4, the further reduction of the amount of catalyst leads to reverse effect. This implies the increase in $T_{CO2,max}$ and even the formation of CO. Exemplarily, for the smallest Fe_2O_3 proportion (0.375 mmol) $T_{CO2,max}$ increases to 400 °C accompanied by broadening of the CO_2 signal and drastic formation of CO; the total yield of CO amounts to 1 mmol. Obviously, the amount of catalyst is no more sufficient to completely oxidise CO originated from soot oxidation. The shift of soot oxidation to higher temperature observed for Fe_2O_3 proportions below 1.25 mmol refers to the reduced number of contact points and catalytic sites involved in oxygen transfer, respectively [14].

3.1.3. Variation of the heating rate

For the investigation of the effect of the heating rate a tight contact mixture of 10 mmol Fe_2O_3 and 5 mmol soot was used. The TPO with the lowest heating rate of 1.8 K/min provides a broad CO_2 trace with a maximum of 0.7 vol.% only, whereas the other heating rates result in sharp CO_2 profiles including higher concentrations of CO_2 (Fig. 5). For instance, when adjusting 3.3 K/min CO_2 evolves with a peak of 7.5 vol.%. The faster soot oxidation is also accompanied by increase in bed temperature of the catalyst/soot mixture enhancing the oxidation rate. Exemplarily, for 10 K/min the maximum rise is approx. 70 K as referred to the inlet temperature, while for 1.8 K/min it is about 25 K only (Fig. 6).

These differences between 1.8 K/min and higher heating rates are related to the temporal input of energy into the packed bed. A slow heating rate leads to slow increase in the temperature of the bed. Contrary, fast heating implies more energy input into the packed bed within the same time, i.e. 0.04 W for 1.8 K/min and 0.08 W for 3.3 K/min referring to a heat capacity of 0.4 J/K for 10 mmol Fe_2O_3, thus causing faster CO_2 production in this period of time. Consequently, the heat production of the exothermic soot oxidation should be intensified by higher heating rates. Nevertheless, the heating rates between 3.3 and 10 K/min surprisingly provide similar CO_2 traces suggesting kinetic limitation of the soot oxidation; just a slight broadening of the CO_2 profile appears. This inhibition is attributed to the drastic decline in

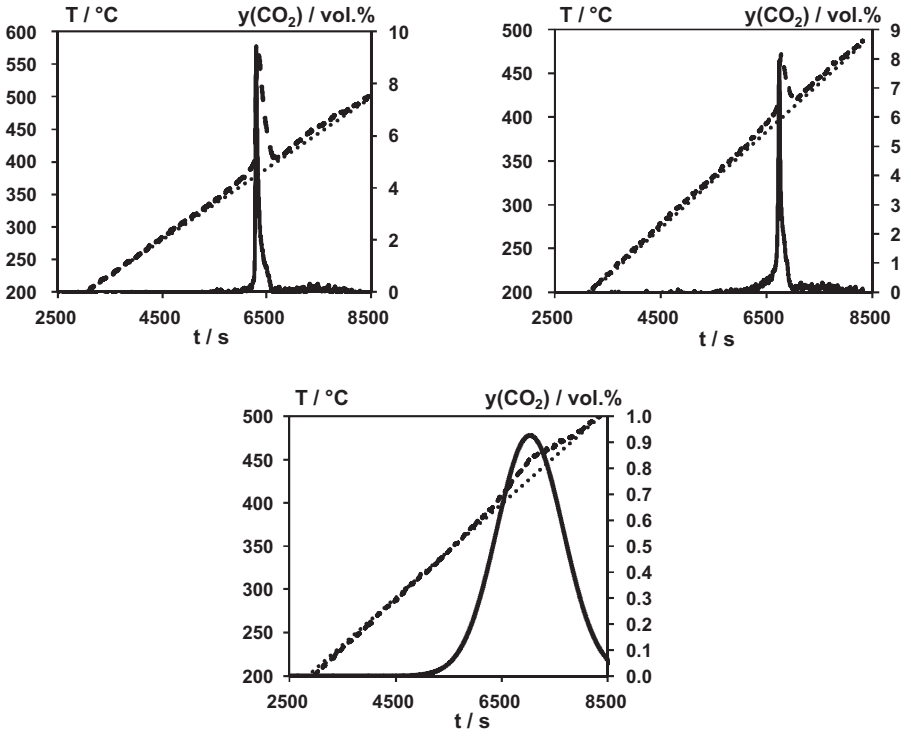

Fig. 3. Temperature profile in the centre of the packed bed (- -) and at the inlet of the reactor (···) as well as CO_2 profile (—) of TPO study performed with Fe_2O_3/soot mixture in tight contact mode: Left, top: 2.5 mmol catalyst. Right, top: 10 mmol catalyst. Bottom, centre: 20 mmol. Conditions: n(soot) = 5 mmol, $y(O_2)$ = 10 vol.%, $y(N_2)$ = 90 vol.%, β = 3.3 K/min, F = 500 ml/min (STP).

gas-phase oxygen. At peak rate of soot oxidation the CO_2 proportion is close to 10 vol.% indicating almost complete consumption of gas-phase O_2. Since the rate of soot oxidation strongly depends on the O_2 content [15], low proportion of oxygen rather decelerates the reaction thus compensating the accelerating effect of the increased heating rate. Limitation of the chemical kinetics by internal and external transfer of mass and heat is to be excluded under the conditions established [24]. Note that the slight broadening of the CO_2 traces plotted versus the temperature is due to the different heating rates. As a consequence, the total amount of CO_2 produced is consistent with the initial amount of carbon used (5 mmol).

3.2. Temperature distribution in the catalyst/soot mixture

Fig. 7 exemplarily shows six images taken by the IR camera upon a TPO investigation performed with a tight contact mixture of 10 mmol Fe_2O_3 and 5 mmol soot (Section 2.2). The pictures refer to different gas inlet temperatures, while the corresponding CO_2 contents are also given. The TPO profile reveals a clear CO_2 peak at 430 °C being close to that reported in Section 3.1. At this inlet temperature the IR camera displays local increase in temperature up to 510 °C implying a rise of 80 K. Moreover, the series of pictures indicates start of heat evolution in the centre of the packed bed and displacement in direction of the outlet as exemplarily indicated for the inlet temperature of 430 °C. This effect is referred

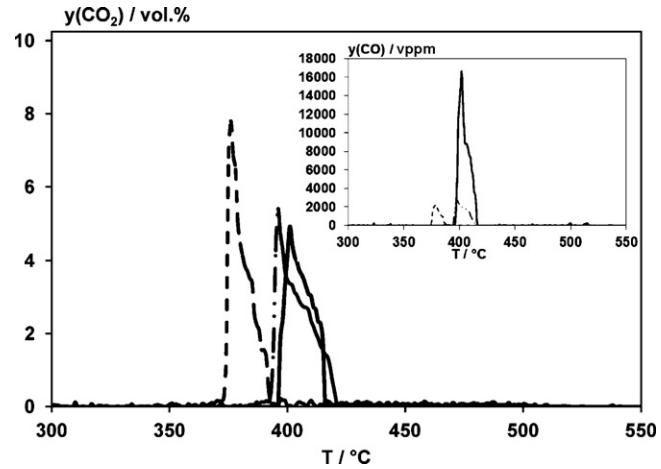

Fig. 4. CO_2 profiles of TPO studies performed with Fe_2O_3/soot mixture in tight contact mode using 1.25 (-.-), 0.625 (—··—) and 0.375 mmol Fe_2O_3 (—). The inlay shows the respective CO evolution. Conditions: $y(O_2)$ = 10 vol.%, $y(N_2)$ = 90 vol.%, β = 3.3 K/min, F = 500 ml/min (STP).

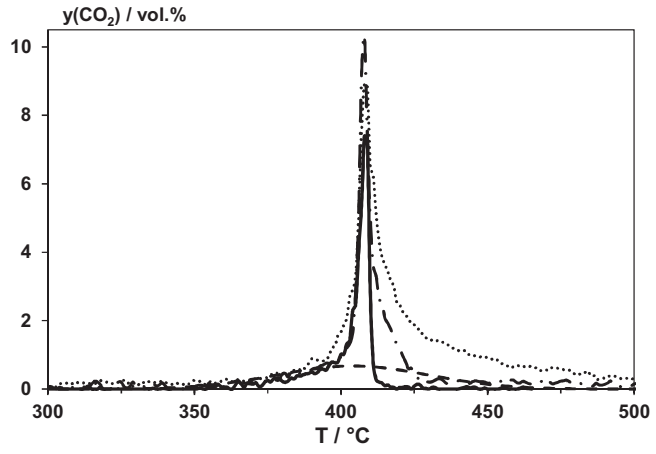

Fig. 5. CO_2 profiles of TPO studies performed with Fe_2O_3/soot mixture in tight contact mode using heating rates of 1.8 (–), 3.3 (—), 5 (—·—) and 10 K/min (···). Conditions: $n(Fe_2O_3)$ = 10 mmol, n(soot) = 5 mmol, $y(O_2)$ = 10 vol.%, $y(N_2)$ = 90 vol.%, F = 500 ml/min (STP).

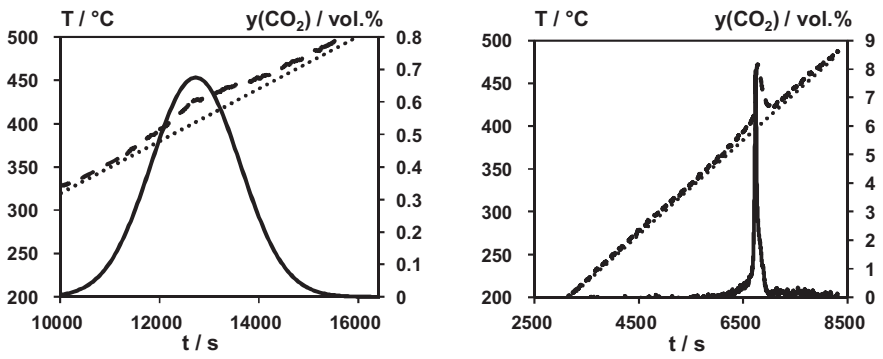

Fig. 6. Temperature profile in the centre of the packed bed (- -) and at the inlet of the reactor (···) and CO_2 profile (—) upon TPO study performed with Fe_2O_3/soot mixture in tight contact mode (left: β = 1.8 K/min, right: β = 10 K/min). Conditions: $n(Fe_2O_3)$ = 10 mmol, n(soot) = 5 mmol, $y(O_2)$ = 10 vol.%, $y(N_2)$ = 90 vol.%, β = 3.3 K/min, F = 500 ml/min (STP).

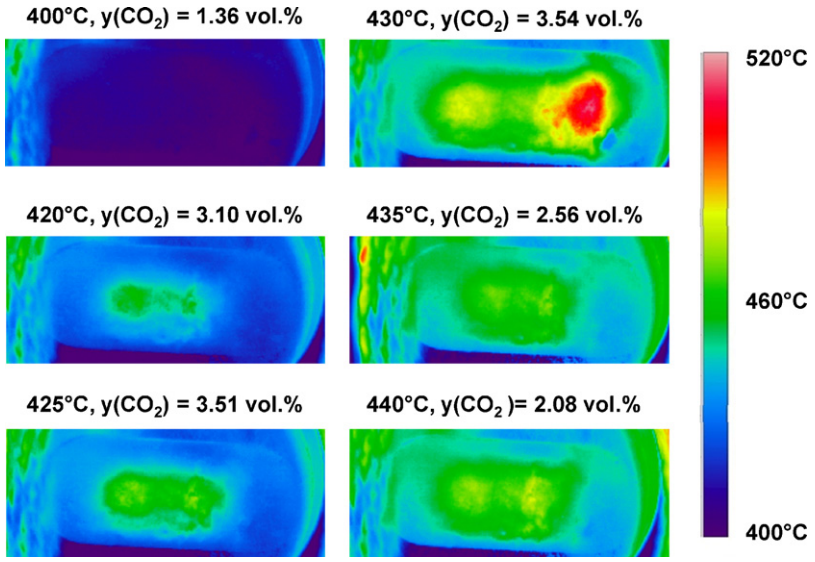

Fig. 7. Distribution of the surface temperature at different inlet temperatures upon TPO performed with Fe_2O_3/soot mixture in tight contact mode. Conditions: $n(Fe_2O_3)$ = 10 mmol, n(soot) = 5 mmol, $y(O_2)$ = 10 vol.%, $y(N_2)$ = 90 vol.%, β = 8.6 K/min, F = 500 ml/min (STP).

to the convection flow of heat, which is also responsible for the absence of any hot spots. Potential relevance of hot spots is reflected by the adiabatic rise in temperature which would amount to ca. 930 °C.

3.3. Isotopic TPO studies with $^{18}O_2$

The isotopic TPO studies were performed to elucidate the role of the Fe_2O_3 catalyst in the transfer of gaseous oxygen to the soot. For the reduction of the amount of $^{18}O_2$ different reaction conditions were established as referred to those used in Section 2.2. Consequently, the resulting CO_2 profiles are different from that obtained above being associated with the slower reaction rate due to reduced O_2 content as well as soot and catalyst amount (Section 2.4). In these isotopic investigations the three possible CO_2 products ($C^{16}O_2$, $C^{18}O$ and $C^{16}O^{18}O$) are monitored and they all reveal several shoulders. The initial formation of carbon dioxide always occurs in the temporal sequence $C^{16}O_2$, $C^{16}O^{18}O$ and $C^{18}O_2$. Furthermore, above 350 °C oxygen exchange between gas-phase and catalyst takes place indicated by the formation of $^{16}O^{18}O$. In the isotopic TPO investigations, $H_2{}^{16}O$, $H_2{}^{18}O$, $C^{16}O$, $C^{18}O$ and $^{16}O_2$ do not form above the limit of the CIMS detector. Based on the TPO and HTPR examinations the molar amounts of ^{18}O and ^{16}O are balanced (Tables 1–3). These calculations show that the quantities of both oxygen isotopes are balanced within the analytical limits (± 9%). Finally, from the respective amounts of ^{16}O present in gaseous products in TPO and the number of $H_2{}^{16}O$ and $H_2{}^{18}O$ formed in HTPR the oxygen exchange degree is derived

Table 1
Molar amounts of oxygen containing species in isotopic TPO of the Fe_2O_3/soot mixture (2:1) in tight contact and in subsequent HTPR. Reaction conditions are presented in Fig. 8.

^{18}O	In		Out	
	Amount (μmol)	Source	Amount (μmol)	Source
TPO	3568	$^{18}O_2$	137	$C^{16}O^{18}O$
			138	$C^{18}O_2$
			2456	$^{18}O_2$
			330	$^{16}O^{18}O$
HTPR	0		796	$H_2{}^{18}O$
Total	3568		3857	
^{16}O	In		Out	
	Amount (μmol)	Source	Amount (μmol)	Source
TPO	1500	Fe_2O_3	137	$C^{16}O^{18}O$
			202	$C^{16}O_2$
			330	$^{16}O^{18}O$
HTPR	0		704	$H_2{}^{16}O$
Total	1500		1373	

Table 2
Molar amounts of oxygen containing species in isotopic TPO of the Fe_2O_3/soot mixture (2:1) in loose contact and in subsequent HTPR. Reaction conditions are presented in Fig. 9.

^{18}O	In		Out	
	Amount (μmol)	Source	Amount (μmol)	Source
TPO	3826	$^{18}O_2$	144	$C^{16}O^{18}O$
			160	$C^{18}O_2$
			2476	$^{18}O_2$
			422	$^{16}O^{18}O$
HTPR	0		669	$H_2{}^{18}O$
Total	3826		3871	
^{16}O	In		Out	
	Amount (μmol)	Source	Amount (μmol)	Source
TPO	1603	Fe_2O_3	144	$C^{16}O^{18}O$
			172	$C^{16}O_2$
			422	$^{16}O^{18}O$
HTPR	0		934	$H_2{}^{16}O$
Total	1603		1672	

representing the fraction of ^{16}O substituted by ^{18}O in the catalyst upon isotopic exposure.

Fig. 8 shows the TPO study of the tight contact mixture composed of 0.6 mmol Fe_2O_3 and 0.3 mmol soot. The major product is $C^{16}O^{18}O$ followed by $C^{16}O_2$ and $C^{18}O_2$. The mass balance of ^{16}O and ^{18}O results in an oxygen exchange degree of 53%.

When the loose contact mixture, which consists of 0.6 mmol Fe_2O_3 and 0.3 mmol soot, is used the isotopic CO_2 features shift to higher temperatures and the soot is not completely consumed even at 1000 °C (Fig. 9, Table 2). The minor performance of the loose contact mixture is basically in line with the results demonstrated in Section 3.1.1. However, like for the tight contact mode $C^{16}O^{18}O$ represents the main product with almost the same total quantity. The level of oxygen exchange is 42%.

Fig. 10 illustrates the results of the isotopic TPO of the tight contact blend of Fe_2O_3 and soot revealing reduced abundance of catalyst (0.15 mmol). It is apparent that the production of carbon dioxide is shifted to lower temperatures as referred to the study with 0.6 mmol Fe_2O_3. Like in Section 3.1.2 this effect is attributed to the lower heat capacity of the packed bed as well as the higher concentration of soot in the Fe_2O_3/soot mixture. Consequently, the produced reaction heat is distributed in quarter volume as compared to 0.6 mmol catalyst. Thus, the local bed temperature is assumed to grow more explaining the increasing rate of soot

Table 3
Molar amounts of oxygen containing species in isotopic TPO of the Fe_2O_3/soot mixture (1:2) in tight contact and in subsequent HTPR. Reaction conditions are presented in Fig. 10.

^{18}O	In		Out	
	Amount (μmol)	Source	Amount (μmol)	Source
TPO	3684	$^{18}O_2$	127	$C^{16}O^{18}O$
			300	$C^{18}O_2$
			2742	$^{18}O_2$
			178	$^{16}O^{18}O$
HTPR	0		415	$H_2{}^{18}O$
Total	3684		3762	
^{16}O	In		Out	
	Amount (μmol)	Source	Amount (μmol)	Source
TPO	649	Fe_2O_3	127	$C^{16}O^{18}O$
			60	$C^{16}O_2$
			178	$^{16}O^{18}O$
HTPR	0		234	$H_2{}^{16}O$
Total	649		599	

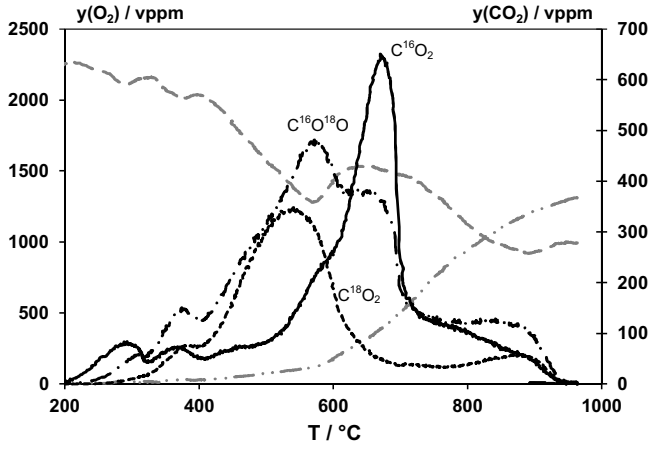

Fig. 8. $C^{18}O_2$ (···), $C^{16}O^{18}O$ (-·-), $C^{16}O_2$ (–), $^{18}O_2$ (--) and $^{16}O^{18}O$ (-···) profiles of isotopic TPO study performed with Fe_2O_3/soot mixture in tight contact mode. Conditions: $n(Fe_2O_3)$ = 0.6 mmol, n(soot) = 0.3 mmol, $y(^{18}O_2)$ = 2270 vppm, N_2 balance, β = 20 K/min, F = 500 ml/min (STP).

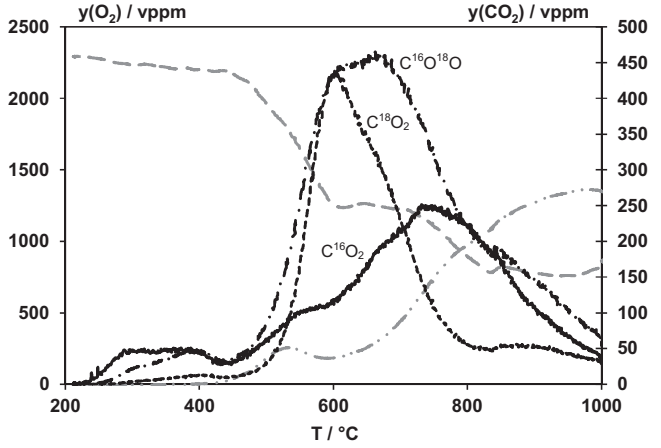

Fig. 9. $C^{18}O_2$ (···), $C^{16}O^{18}O$ (-·-), $C^{16}O_2$ (–), $^{18}O_2$ (--) and $^{16}O^{18}O$ (-···) profiles of isotopic TPO study performed with Fe_2O_3/soot mixture in loose contact mode. Conditions: $n(Fe_2O_3)$ = 0.6 mmol, n(soot) = 0.3 mmol, $y(^{18}O_2)$ = 2270 vppm, N_2 balance, β = 20 K/min, F = 500 ml/min (STP).

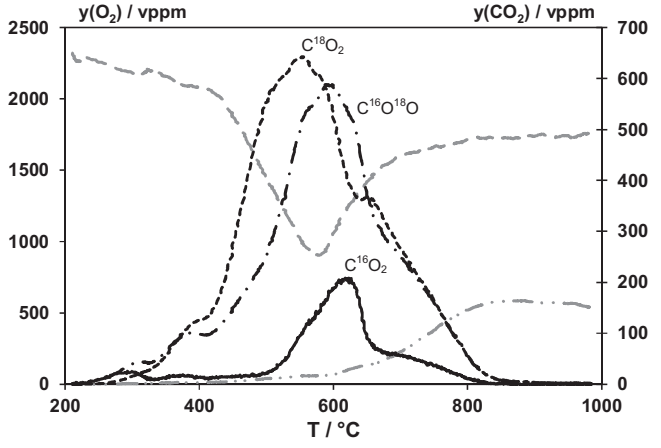

Fig. 10. $C^{18}O_2$ (···), $C^{16}O^{18}O$ (-·-), $C^{16}O_2$ (–), $^{18}O_2$ (--) and $^{16}O^{18}O$ (-···) profiles of isotopic TPO study performed with Fe_2O_3/soot mixture in tight contact mode. Conditions: $n(Fe_2O_3)$ = 0.15 mmol, n(soot) = 0.3 mmol, $y(^{18}O_2)$ = 2270 vppm, N_2 balance, β = 20 K/min, F = 500 ml/min (STP).

oxidation. Moreover, Table 3 shows that in contrast to the TPO with 0.6 mmol Fe_2O_3 $C^{18}O_2$ forms as the major product, while $C^{16}O_2$ appears only in rather small abundance. The mass balance indicated the degree of oxygen exchange to be 64%.

3.4. Reaction mechanism of the soot oxidation on Fe_2O_3 catalyst

For the interpretation of the isotopic TPO studies a mechanistic model of the soot oxidation on Fe_2O_3 catalyst is set up which is based on global reactions. In line with literature [13,14] this scheme implies the transfer of oxygen chemisorbed on active Fe surface sites (Fe(^{x}O)) to the soot via physical contact points to be a crucial step. This release of oxygen results in partially reduced Fe sites denoted as Fe(*). The transferred oxygen species finally stick on active soot sites (CC_f) to form oxygen containing surface complexes (C(C^{x}O)), e.g. ether and carbonyl groups (Eqs. (1) and (2)). Their decomposition leads to the production of gaseous $C^{16}O$ and $C^{18}O$ as well as new active C sites (C_f) (Eqs. (3) and (4)). Basically, the oxygen transfer might also result in the formation of C(C^xO_2) surface species, such as lactones and anhydrides, which decompose to yield C^xO_2 [4]. C($C^{16}O$) and C($C^{16}O_2$) species are initially present on the soot surface of the soot used, but their abundance of about 0.01 mmol is rather insignificant as compared to the entire amount of soot consumed (0.3 mmol). Moreover, terminal C(CH) groups are not accounted for the model due to the high molar C/H ratio of the soot employed amounting to ca. 14.

$$CC_f + Fe(^{16}O) \rightarrow C(C^{16}O) + Fe(*) \quad (1)$$

$$CC_f + Fe(^{18}O) \rightarrow C(C^{18}O) + Fe(*) \quad (2)$$

$$C(C^{16}O) \rightarrow C^{16}O(g) + C_f \quad (3)$$

$$C(C^{18}O) \rightarrow C^{18}O(g) + C_f \quad (4)$$

The surface vacancies of the catalyst originated from the oxygen transfer can be refilled by gaseous $^{18}O_2$ and $^{16}O^{18}O$ and (Eqs. (5) and (6)). The participation of $^{16}O^{18}O$ has to be considered above 350 and 450 °C (depending on the amount of catalyst) as these temperatures cause substantial oxygen exchange of gas-phase and surface oxygen (Eq. (7)) [25]; the reaction of $^{16}O^{18}O$ with Fe(^{16}O) into $^{16}O_2$ represents a negligible route, since the latter was not found. However, it is unlikely that only the Fe sites close to the contact points are supplied by gas-phase oxygen. We rather assume that the Fe(*) vacancies are mainly regenerated by surface oxygen chemisorbed on neighbouring Fe sites, i.e. Fe(^{x}O) species, thus forming a cascade of production and refilling of surface vacancies [13,14]. Final regeneration occurs at certain distance to the contact points according to Eq. (5).

$$^{18}O_2(g) + 2Fe(*) \rightarrow 2Fe(^{18}O) \quad (5)$$

$$^{16}O^{18}O(g) + 2Fe(*) \rightarrow Fe(^{16}O) + Fe(^{18}O) \quad (6)$$

$$^{18}O_2(g) + Fe(^{16}O) \rightleftharpoons Fe(^{18}O) + {}^{16}O^{18}O(g) \quad (7)$$

As another mechanism for the refilling of surface vacancies diffusing bulk oxygen ($^{16}O_{bulk}$) has to be considered (Eq. (8)). The HTPR investigations directly performed after TPO show marked evolution of $H_2{}^{18}O$ substantiating the involvement of crystalline oxygen. This is exemplarily estimated for the catalyst amount of 0.6 mmol (tight contact); for complete coverage of the Fe_2O_3 surface by spherical O atoms (d = 0.14 nm [26]) a quantity of 31 μmol oxygen is required. Hence, the proportion of 796 μmol ^{18}O evolved in HTPR in the form of water (Table 1) clearly exceeds the abundance of surface oxygen estimated for a monolayer thus proving the participation of bulk O. The refilling of surface vacancies by bulk oxygen produces again vacancies in the crystalline lattice denoted as $(*)_{bulk}$. These bulk vacancies can be regenerated by adjacent lattice oxygen (Eq. (9)), whereas final regeneration is achieved by transfer of surface oxygen, i.e. Fe(^{16}O) and Fe(^{18}O). This implies exchange of ^{16}O by ^{18}O in the crystalline lattice of the Fe_2O_3 catalyst and partial recycling of ^{16}O originally released from the catalyst, e.g. when Fe(^{16}O) forms according to Eq. (6).

As a consequence of the participation of bulk ^{16}O species, it is obvious that the decrease in the amount of catalyst from 0.6 to 0.15 mmol results in lower quantity of $C^{16}O_2$ totally formed in TPO (30 μmol vs. 101 μmol), i.e. less catalyst directly corresponds to smaller number of surface and bulk ^{16}O species involved. In reversal conclusion, for 0.15 mmol Fe_2O_3 the overall quantity of $C^{18}O_2$ is significantly increased (150 μmol vs. 101 μmol for 0.6 mmol Fe_2O_3).

$$^{16}O_{bulk} + Fe(*) \rightarrow Fe(^{16}O) + (*)_{bulk} \quad (8)$$

$$(*)_{bulk} + {}^{16}O_{bulk} \rightarrow {}^{16}O_{bulk} + (*)_{bulk} \quad (9)$$

The driving force of the transfer of oxygen from the catalyst to the soot is considered to be the formation of CO_x which includes cycles of partial reduction and re-oxidation of the catalyst. As a case study we calculate the free reaction enthalpy ($\Delta_f G$) (T = 500 K, p = 1 bar) of the reaction of Fe_2O_3 with carbon to CO_2 ($\Delta_f G$ = −56 kJ/mol) and subsequent re-oxidation of the formed Fe_3O_4 by gaseous O_2 ($\Delta_f G$ = −338 kJ/mol) [27]. Both reactions are spontaneous, whereas the overall free enthalpy is equal to that of the carbon oxidation by O_2 ($\Delta_f G$ = −394 kJ/mol).

Contrary, no significant thermal release of oxygen occurs in the absence of the soot, for instance in O_2-TPD [15,20,24]. These results show that the presence of the reducing agent soot is necessarily required for the release and uptake of oxygen by the catalyst. It should be noted that in the solid–solid reaction of Fe_2O_3 and soot performed under tight contact conditions in N_2 flow the iron oxide transfers oxygen even at temperatures below 250 °C [14,24].

The progressive formation of $C^{16}O_2$, $C^{16}O^{18}O$ and $C^{18}O_2$ in the initial phase of TPO indicates that rather surface or sub-surface oxygen of Fe_2O_3 is firstly involved. We interpret this sequence with the transfer of oxygen by Fe(^{16}O) sites at the contact points accompanied by refilling of Fe(*) vacancies by gaseous oxygen according to Eq. (5). This process results in continuous replacement of surface ^{16}O by ^{18}O leading to formation of $C^{16}O^{18}O$ and finally $C^{18}O_2$. The re-oxidation rate of Fe(*) sites by bulk oxygen (Eq. (8)) seems to be slower as compared to that of surface and gas-phase oxygen, respectively (Eq. (5)). This is indicated by the $C^{16}O_2$ peak being located at the highest temperatures among the C^xO_2 species in all the isotopic experiments. Reddy and Cooper [28] provided a comparison of the mobility of crystalline and surface oxygen upon exposure of a Fe_2O_3 single crystal to $^{18}O_2$. Estimation of the respective diffusion coefficients for 450 °C in a catalyst particle with a typical size of ca. 10^{-6} m oxygen to 450 °C leads to K = ca. 10^{-12} s^{-1} for surface exchange by adsorption and surface diffusion and to D = ca. 10^{-43} s^{-1} for bulk diffusion in the catalyst. These values show that surface exchange and surface diffusion, respectively, is much fast than bulk diffusion. It should be mentioned that the oxygen transfer of the catalyst is maintained even up to high soot conversion levels of 90% [14]. This feature is substantiated by the continuous formation of ^{16}O containing carbon dioxide upon TPO. Furthermore, it is tentatively discernible that tight contact mode, which is characterised by increased number of contact points between Fe_2O_3 and soot, provides more bulk oxygen than loose contact does being reflected by the higher oxygen exchange level (53% vs. 42%) and the greater total quantity of $C^{16}O_2$ (101 μmol vs. 86 μmol, Tables 1 and 2).

Furthermore, another route of oxygen exchange has to be taken into consideration which takes place by adsorption and desorption of CO_2 via carbonate surface complexes denoted as Fe(CO_3) (Eqs. (10) and (11)) [20]. Depending on the chemisorption of $C^{16}O_2$ or $C^{18}O_2$ on Fe(^{16}O) or Fe(^{18}O) sites an exchange of surface ^{18}O by ^{16}O

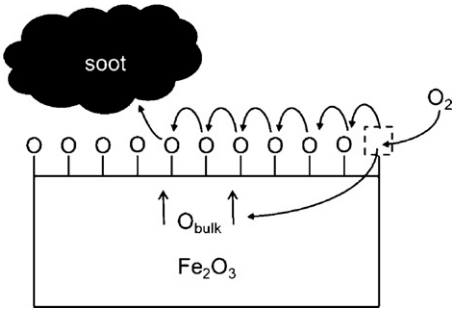

Fig. 11. Scheme of the mechanism of catalytic soot oxidation on Fe_2O_3.

released from carbon dioxide or vice versa is possible. In very similar way the oxygen exchange occurs by chemisorption of $C^{16}O^{18}O$ on Fe(^{16}O) and Fe(^{18}O), respectively, followed again by carbonate decomposition.

$$C^{16}O_2(g) + Fe(^{18}O) \rightleftharpoons Fe(C^{16}O_2{}^{18}O) \rightleftharpoons C^{16}O^{18}O(g) + Fe(^{16}O) \quad (10)$$

$$C^{18}O_2(g) + Fe(^{16}O) \rightleftharpoons Fe(C^{18}O_2{}^{16}O) \rightleftharpoons C^{16}O^{18}O(g) + Fe(^{18}O) \quad (11)$$

In the three isotopic TPO examinations no significant difference in the total evolution of $C^{16}O^{18}O$ exists ranging from 127 μmol to 142 μmol (Tables 1–3). This implies that the type of contact mode does not affect the entire quantity of $C^{16}O^{18}O$. We therefore suppose that the major part of $C^{16}O^{18}O$ is attributed to the oxygen exchange by surface carbonate described by Eqs. (10) and (11).

Like in Section 3.1 the absence of gaseous C^xO in the TPO investigation is associated with the high oxidation activity of the Fe_2O_3 catalyst [20]. In the isotopic experiment carbon dioxide originated from the catalytic oxidation of C^xO is produced in the form of $C^{16}O_2$, $C^{16}O^{18}O$ and $C^{18}O_2$ depending on the oxygen isotope involved as exemplarily shown in Eq. (12).

$$C^{16}O(g) + Fe(^{16}O) \rightarrow C^{16}O_2(g) + Fe(*) \quad (12)$$

The global reactions discussed above give a qualitative explanation for the formation of $C^{16}O_2$, $C^{16}O^{18}O$ and $C^{18}O_2$. It should be noticed that this model does consider the non-catalytic oxidation of soot [29] to be a major route, since the bare soot used starts oxidising at significantly higher temperatures.

4. Conclusions

Based on the experiments and discussions presented in this paper we conclude a scheme of global reactions describing the mechanism of the catalytic soot oxidation on Fe_2O_3. According to this scheme illustrated in Fig. 11 oxygen is transferred from the catalyst surface to the soot by contact points. The resulting oxygen defects of the catalyst surface are refilled either by surface migration and final re-oxidation by gas-phase oxygen, respectively, or by diffusing bulk oxygen. The oxygen deficiency of the lattice is balanced by migration of oxygen from the surface or sub-surface to the bulk of the catalyst.

Furthermore, the heat capacity of the catalyst reveals strong effect on the heat evolution upon soot oxidation thus affecting the local temperature and the rate of soot oxidation. Hence, for maximum soot oxidation rate an optimum mass of catalyst is required. Additionally, high catalytic activity is closely related to a sufficient amount of contact points between Fe_2O_3 and soot.

Acknowledgements

We thankfully acknowledge the cooperation and financial support of Umicore (Hanau).

References

[1] P. Zelenka, W. Cartellieri, P. Duke, Applied Catalysis B 7 (1996) 3.
[2] A. Setiabudi, B.A.A.L.v. Setten, M. Makkee, J.A. Moulijn, Applied Catalysis B 35 (2002) 159.
[3] M. Crocoll, S. Kureti, W. Weisweiler, Journal of Catalysis 229 (2005) 480.
[4] A. Setiabudi, M. Makkee, J.A. Moulijn, Applied Catalysis B 50 (2004) 185.
[5] O. Salvat, P. Marez, G. Belot, SAE Technical Paper Series 2000-01-0473.
[6] B.A.A.L.v. Setten, J.M. Schouten, M. Makkee, J.A. Moulijn, Applied Catalysis B 28 (2000) 253.
[7] E. Aneggi, C.d. Leitenburg, G. Dolcetti, A. Trovarelli, Catalysis Today 114 (2006) 40.
[8] A. Bueno-López, K. Krishna, M. Makkee, J.A. Moulijn, Journal of Catalysis 230 (2005) 237.
[9] J.v. Doorn, J. Varloud, P. Mériaudeau, V. Perrichon, Applied Catalysis B 1 (1992) 117.
[10] J. Oi-Uchisawa, A. Obuchi, Z. Zhao, S. Kushiyama, Applied Catalysis B 18 (1998) 183.
[11] J. Oi-Uchisawa, S. Wang, T. Nanba, A. Ohi, A. Obuchi, Applied Catalysis B 44 (2003) 207.
[12] S.B. Simonsen, S. Dahl, E. Johnson, S. Helveg, Journal of Catalysis 255 (2008) 1.
[13] G. Mul, F. Kapteijn, C. Doornkamp, J.A. Moulijn, Journal of Catalysis 179 (1998) 258.
[14] D. Reichert, H. Bockhorn, S. Kureti, Applied Catalysis B 80 (2008) 248.
[15] D. Reichert, T. Finke, N. Atanassova, H. Bockhorn, S. Kureti, Applied Catalysis B 84 (2008) 803.
[16] Z. Zhang, D. Han, S. Wei, Y. Zhang, Journal of Catalysis 276 (2010) 16.
[17] S. Kureti, K. Hizbullah, W. Weisweiler, Applied Catalysis B 3 (2003) 281.
[18] P. Balle, H. Bockhorn, B. Geiger, N. Jan, S. Kureti, D. Reichert, T. Schröder, Chemical Engineering and Processing 45 (2006) 1065.
[19] D. Reichert, Untersuchungen zur Reaktion von Stickstoffoxiden und Sauerstoff am Katalysator α-Fe_2O_3, Ph.D. Thesis, University of Karlsruhe, 2008.
[20] S. Wagloehner, D. Reichert, D. Leon-Sorzano, P. Balle, B. Geiger, S. Kureti, Journal of Catalysis 260 (2008) 305.
[21] J.P.A. Neeft, O.P.V. Pruissen, M. Makkee, J.A. Moulijn, Applied Catalysis B 12 (1997) 21.
[22] G. Mul, J.P.A. Neeft, F. Kapteijn, J.A. Moulijn, Carbon 36 (1997) 1269.
[23] J.P.A. Neeft, F. Hoornaert, M. Makkee, J.A. Moulijn, Thermochimica Acta 287 (1996) 261.
[24] S. Wagloehner, Soot oxidation on iron oxide catalysts, Ph.D. Thesis, Karlsruhe Institute of Technology, 2012.
[25] J. Novakova, Catalysis Reviews 4 (1971) 77.
[26] T. Klos, Eindimensionale-Multikomponenten-Raman-Streuung zur Messung charakteristischer Turbulenzeigenschaften, VDI-Reihe 8, Fortschr.-Ber. Nr. 692 (1998).
[27] W.M. Haynes, Handbook of Chemistry and Physics, 2011.
[28] K.P.R. Reddy, A.R. Cooper, Journal of the American Ceramic Society 66 (1983) 664.
[29] K. Sendt, B.S. Haynes, Journal of Physical Chemistry C 111 (2007) 5465.